Check for updates

Aggregation-Induced Emissive Scintillators: A New Frontier for Radiation Detection and Imaging

Xinyi Li[1], Jiafu Yu[1], Yinghao Fan[1], Yuting Gao[1,2] ✉, Guangda Niu[3] ✉

HIGHLIGHTS

- Summarizes the high quantum efficiency and rapid response of aggregation-induced emission (AIE) materials in radiation detection, showcasing their advantages in high-energy radiation signal detection.

- Reviews the progress in AIE materials' radiation response for efficient detection of X-rays, γ rays, neutrons, and other radiation types.

- Long term stability, device integration, and adaptability to diverse radiation forms remain key challenges for broader AIE material applications.

ABSTRACT Aggregation-induced emission (AIE) is a unique phenomenon where certain organic materials exhibit enhanced luminescence in their aggregated states, overcoming the typical quenching observed in conventional organic materials. Since its discovery in 2001, AIE has driven significant advances in fields like OLEDs and biological imaging, earning recognition in fundamental research. However, its application in high-energy radiation detection remains underexplored. Organic scintillators, though widely used, face challenges such as low light yield and poor radiation attenuation. AIE materials offer promising solutions by improving light yield, response speed, and radiation attenuation. This review summarizes the design strategies behind AIE scintillators and their very recent applications in X-ray, γ-ray, and fast neutron detection. We highlight their advantages in enhancing detection sensitivity, reducing background noise, and achieving high-resolution imaging. By addressing the current challenges, we believe AIE materials will play a pivotal role in advancing future radiation detection and imaging technologies.
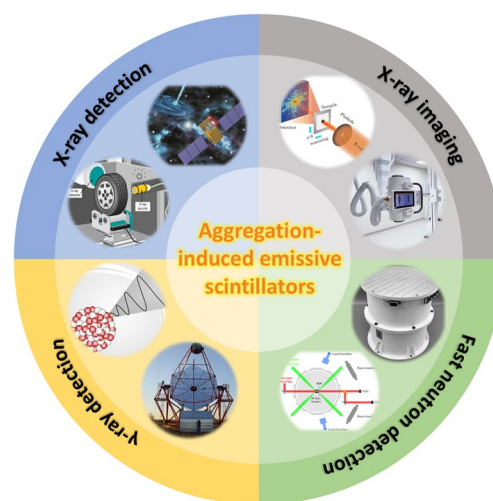
KEYWORDS Aggregation-induced emission; Scintillators; Radiation detection; Radiation imaging

✉ Yuting Gao, gaoyt@cug.edu.cn; Guangda Niu, guangda_niu@hust.edu.cn

[1] Engineering Research Center of Nano-Geomaterials of Ministry of Education, Faculty of Material Science and Chemistry, China University of Geosciences, Wuhan 430074, People's Republic of China

[2] State Key Laboratory of Biocatalysis and Enzyme Engineering, School of Life Sciences, Hubei University, Wuhan 430062, People's Republic of China

[3] Wuhan National Laboratory for Optoelectronics and School of Optical and Electronic Information, Huazhong University of Science and Technology, Wuhan 430074, People's Republic of China

1 Introduction

Radiation detection and imaging technologies are widely utilized in fields such as medical diagnostics [1], high-energy physics, non-destructive testing [2, 3], and security surveillance [4]. Central to these technologies are radiation detectors, which convert radiation into measurable signals [5]. Scintillator-based radiation detection is the most widely used approach today, owing to the fast response speed, ease of fabrication, integration capability, and low cost of scintillators [6]. Scintillation is the process by which ionizing radiation interacts with scintillator materials to produce photons [7]. The ongoing goal in this field is to develop scintillators with higher efficiency and faster timing properties. Higher efficiency allows for the generation of more photons from a given radiation dose, improving image quality without increasing patient exposure. Fast scintillation not only enables quicker imaging with less lag, but also plays a crucial role in applications such as computed tomography (CT), positron emission tomography (PET), and high-energy physics experiments [8–10].

The development of radiation detection scintillators dates back to the late nineteenth century, with early advancements such as calcium tungstate ($CaWO_4$) and zinc sulfide (ZnS)-based powders that efficiently convert X-rays into visible light [11, 12]. Since then, various inorganic single crystals and powders have been developed, many of which exhibit outstanding performance and are now widely used. While inorganic scintillators are known for their high light yield and effectiveness in detecting high-energy radiation, they still face several challenges. For example, common scintillators like NaI and CsI are prone to instability due to their hygroscopic nature [13, 14]. Achieving both high sensitivity and temporal resolution is also difficult. Scintillators like BaF_2 offer high temporal resolution but suffer from low exciton utilization, reducing X-ray sensitivity [15]. Meanwhile, rare-earth-based scintillators like SrI_2 have high exciton utilization but slow d→f transitions, limiting their temporal resolution [16]. Additionally, doped ion-based scintillators, such as CsI, often experience lattice defects, leading to prolonged afterglow and reduced temporal resolution [17]. Overcoming these challenges is essential to enhancing scintillator performance for radiation detection.

In recent years, organic scintillators have gained significant attention due to their advantages, including low-cost raw materials, ease of modification and processing, and the potential for large-area fabrication, making them highly promising for applications in radiation detection and imaging. However, traditional planar-structured organic scintillators often suffer from reduced emission intensity caused by π-π stacking interactions in the solid and aggregated states, which negatively impact their radiation detection performance [18]. The discovery of the aggregation-induced emission (AIE) phenomenon by Tang and colleagues has fundamentally changed the fundamental understanding of photoluminescence in organic compounds [19]. Unlike the aggregation-caused quenching (ACQ) effect, which leads to a decrease in emission intensity when many luminescent materials aggregate, AIE materials exhibit enhanced light emission in the aggregated state. This breakthrough has opened up exciting possibilities for research in organic electronics, including light-emitting diodes [20–22], sensors [23, 24], and other advanced technologies. However, despite its substantial progress, the application of AIE materials in high-energy radiation detection remains a largely untapped area.

Very recently, a range of AIE-based scintillators has been studied for potential application of radiation detection and imaging. These scintillators offer several advantages, including enhanced detection sensitivity, reduced background noise, and high-resolution imaging. This review will explore the working principles and design strategies of AIE materials, examining their applications in the detection of X-rays, γ-rays, and fast neutrons, as well as in radiation imaging technologies. Additionally, the review will address the opportunities and challenges associated with AIE scintillators in radiation detection and imaging, highlighting potential directions for future development (Fig. 1).

2 Design Strategy of Aggregation-Induced Emission Scintillators

As shown in Fig. 2a, the core mechanism underlying AIE is the restriction of intramolecular motion (RIM) [25, 26]. A key component of the RIM mechanism is the restriction of intramolecular rotation (RIR), which notably affects flexible units such as benzene rings and alkenes. In solution, the free rotation of these units results in energy dissipation, while in the aggregated state, steric hindrance or intermolecular stacking restricts rotational motion, thereby minimizing non-radiative decay. Similarly, the restriction of intramolecular vibration (RIV) reduces non-radiative relaxation in the aggregated state by limiting the vibrational
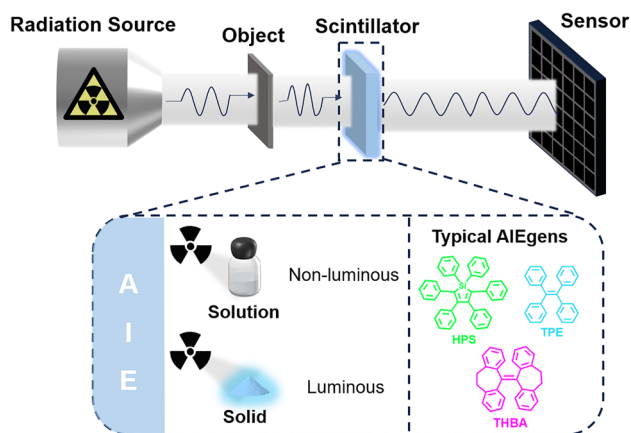
Fig. 1 Aggregation-induced luminescent scintillators for radiation detection and imaging applications

degrees of freedom. Furthermore, AIE-active molecules are specifically designed to avoid detrimental π-π stacking interactions, which are commonly associated with fluorescence quenching in aggregated systems. Instead, these molecules preferentially engage in weaker interactions, such as C–H…π, even in the aggregated state, effectively preventing the fluorescence quenching typically observed in ACQ processes. Collectively, these factors contribute to the enhanced luminescent efficiency of AIE molecules in their aggregated form.

Building on this core mechanism, the design of AIE molecules requires careful consideration of molecular structures to optimize the RIM effect. As illustrated in Fig. 2b, the process begins with the selection of core fluorophores that exhibit strong fluorescence in their monomeric state. These fluorophores typically consist of conjugated π-electron
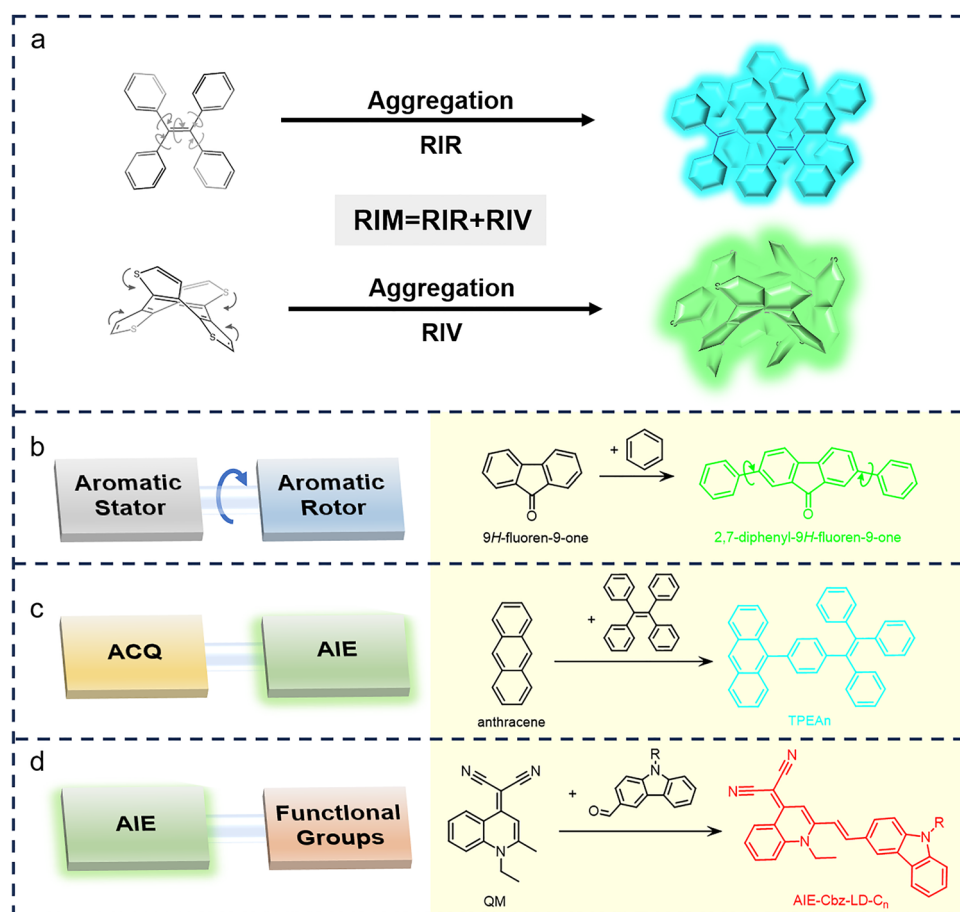

Fig. 2 a As shown above, tetraphenylethylene (TPE) is non-emissive when dissolved, but becomes emissive on polymerisation due to the restriction of intramolecular rotation (RIR). In the figure below, cyclooctyl tetrathiophene (COTh) shows AIE activity in the aggregated state due to restriction by intramolecular vibration (RIV). **b–d** Schematic diagram for constructing an AIE molecule

systems, such as benzene, naphthalene, anthracene, or BODIPY, which are capable of absorbing light and re-emitting it as fluorescence [27]. However, in solution, these fluorophores often demonstrate weak or negligible fluorescence due to non-radiative decay processes, such as the rotational or vibrational motions of flexible molecular segments.

To overcome this fluorescence quenching in solution, the design of AIE molecules typically involves the incorporation of rigid or bulky substituents, such as aromatic rings, alkyl chains, or extended aromatic fragments. These substituents play a crucial role in restricting the internal flexibility of the molecules. Specifically, rotatable single bonds linking rigid aromatic "stators" with flexible "rotors" introduce a non-planar structure. The twisted geometry of the rotors prevents the close π-π stacking interactions between adjacent luminophores, thereby avoiding fluorescence quenching in the aggregated state. This structural modification effectively suppresses non-radiative decay processes in the aggregated form, as the restricted motion of the molecular segments prevents excited-state energy from dissipating through rotational or vibrational motions, thus enabling more efficient radiative decay [28]. A notable example of this strategy is the work by Wang's research group, where two phenyl rings were attached to fluorenone to create an AIE luminophore (Fig. 2b) [29]. This luminophore shows negligible emission in solution but exhibits bright green fluorescence in the crystalline state.

Similarly, the chemical modification of ACQ scaffolds by incorporating AIE-active groups can lead to the development of new AIE materials (Fig. 2c). For instance, Tang's research group introduced freely rotating tetraphenylethylene (TPE) into the traditional ACQ molecule anthracene [30]. This modification restricts intramolecular rotation, resulting in the molecule TPEAn exhibiting aggregation-induced emission (AIE) behavior in the condensed phase. Furthermore, chemical modifications of AIE molecules, such as the incorporation of functional groups, the integration of AIE units into polymer backbones or side chains, or the embedding of AIE-active molecules into host–guest systems, offer alternative strategies for the design of novel AIE materials (Fig. 2d) [31]. A notable example is the work by Zhu and colleagues, who synthesized a series of AIE fluorescent probes, AIE-Cbz-LD-C_n, by conjugating quinoline with carbazole as the core unit [32]. The inclusion of the QM group

in AIE-Cbz-LD-C_n imparts strong AIE activity, highlighting the versatility of these modifications. These strategies significantly enhance the applicability of AIE compounds, enabling their use in a wide range of applications, including sensors, optoelectronic devices, and imaging technologies.

The unique luminescent properties of AIE materials enable their potential use in radiation detection and imaging technologies. For effective detection of X-rays and γ-rays, materials must interact efficiently with these high-energy photons through either absorption or scattering, and subsequently convert the absorbed energy into a detectable signal. Therefore, the design of AIE molecules with conjugated π-systems is essential for enhancing the absorption of high-energy X-ray and γ photons. Conjugation promotes electronic delocalization within the molecule, which improves charge transport and enhances the material's ability to interact with ionizing radiation, thereby facilitating energy transfer and boosting luminescent efficiency [33]. Furthermore, heavy atoms with high atomic numbers are known to possess stronger photon absorption and scattering capabilities [34, 35]. Thus, incorporating heavy atoms such as halogens or metals into scintillation materials can further enhance their ability to absorb X-ray photons, improving the overall detection performance of the scintillators.

The detection mechanism for fast neutrons differs significantly from that of X-rays and γ-rays. Unlike these high-energy photons, fast neutrons do not interact directly with electrons to produce electromagnetic radiation [36]. Instead, they primarily interact with matter through nuclear reactions. To detect fast neutrons, organic materials must efficiently convert the neutrons' kinetic energy into secondary particles or radiation. Therefore, the incorporation of hydrogen-rich units in AIE molecules is essential for enhancing neutron detection. Since hydrogen atoms have a mass similar to that of neutrons, they are particularly effective in elastic scattering events. This enables the transfer of the neutron's kinetic energy to hydrogen atoms, which then emit secondary radiation, facilitating detection.

Through these strategies, the design of AIE materials can be optimized for different types of radiation detection, enhancing X-ray and γ-ray detection efficiency through improved photon absorption, or boosting fast neutron detection efficiency by incorporating hydrogen-rich structures. This targeted design approach enables AIE materials

to possess broad application potential in the fields of radiation detection and imaging.

3 Application of AIE Scintillators in X-Ray Detection and Imaging

3.1 X-Ray Detection

AIE materials have garnered significant attention as scintillators for X-ray detection, primarily due to their efficient conversion of X-ray energy into visible light. These materials offer advantages such as high light yields, low detection limits, and a competitive edge over traditional scintillators. Recent advancements further demonstrate their potential to enhance X-ray detection capabilities and drive progress in radiation imaging technologies. In the following section, we highlight key developments in AIE-based scintillators, emphasizing their innovative contributions to the field.

One notable advancement is in hydroxyphenyl silane (HPS) crystals, which emit a strong peak at 490 nm under X-ray excitation, with a scintillation decay time of 21 ns and a light yield of 11,000 photons MeV^{-1} (Fig. 3a, b) [37]. Researchers have further optimized these materials by doping HPS into poly(vinylcarbazole) (PVK), creating a series of plastic scintillators with varying concentrations of HPS (as shown in Fig. 3c). At HPS concentrations of 0.50 and 1.0 mol%, these scintillators achieve a scintillation light yield of 8200 photons MeV^{-1}, demonstrating the tunability of AIE materials for improved performance in X-ray detection [38].

The effectiveness of X-ray detection is heavily influenced by the atomic composition of the materials used. Materials with higher atomic numbers typically exhibit superior X-ray absorption and attenuation efficiencies. One approach to further enhance the X-ray absorption capability and luminescence intensity of AIE materials is the introduction of heavy atoms, such as halogen doping,
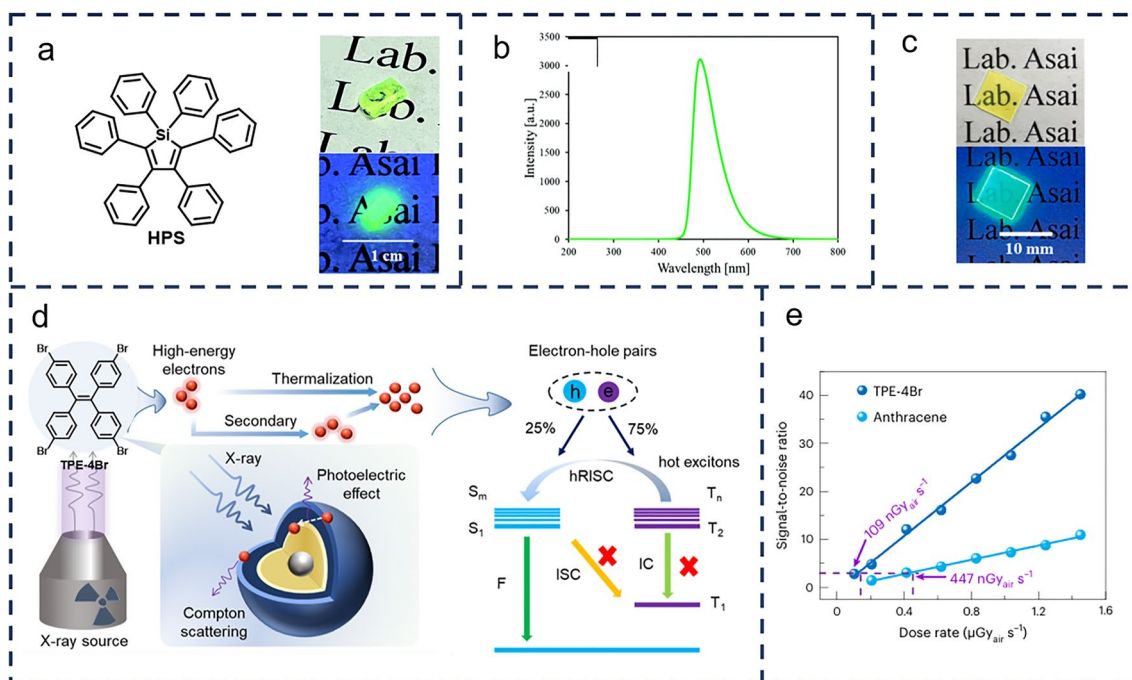

Fig. 3 **a** Physical images of the molecular structure and crystals of HPS under natural light and UV light; **b** XRL spectra of HPS crystals. (**a** and **b** Reproduced with permission from Ref. [37] Copyright 2022 the Partner Organizations). **c** Photographs of synthetic plastic scintillators prepared using HPS under visible light (top) and UV ($\lambda = 302$ nm) irradiation (bottom). (**c** Reproduced with permission from Ref. [38] Copyright 2023 Elsevier B.V.). **d** Schematic representation of the X-ray induced scintillation process in a TPE-4Br thermal exciton scintillator. h, hole; e, electron; F, fluorescence; ISC, intersystem crossing. **e** Signal-to-noise ratio as a function of the dose rate for TPE-4Br and anthracene. (**d** and **e** Reproduced with permission from Ref. [39] Copyright 2024 Nature)

which can significantly improve detection sensitivity. For example, Du et al. [39] developed a novel strategy to create highly efficient and ultra-fast organic scintillators. By directing all thermal excitons into a rapid singlet emission state—bypassing the lowest triplet state—they synthesized 1,1,2,2-tetraphenylethylene(4-bromophenyl) (TPE-4Br) (Fig. 3d). This scintillator exhibits remarkable properties, including an ultra-fast radiative lifetime, high light yield, and enhanced X-ray absorption efficiency. Notably, TPE-4Br demonstrated a minimum detection limit of 109 nGy s^{-1}, which is 50 times lower than the conventional dose rate required for medical diagnoses (5.5 μGy s^{-1}), highlighting its potential for highly sensitive X-ray detection (Fig. 3e).

In a different approach, Shonde et al. [40] further advanced the field by combining high-Z metal halide anions with highly luminescent AIE organic cations to create robust organic–inorganic hybrid systems. These hybrid systems, unlike the halogen-doped systems discussed earlier, exhibit both enhanced X-ray absorption and rapid sensitized radioluminescence. They synthesized the one-dimensional organic metal halide (TPA-P)$_2$ZnBr$_4$ (Fig. 4a), which demonstrated an absolute light yield of (14,700 ± 800) photons MeV^{-1} and a decay lifetime of 9.96 ns. As illustrated in Fig. 4b, this organic metal halide hybrid scintillator also showed a low detection limit of 21.3 nGy s^{-1} and excellent response linearity over a broad range of X-ray dose rates. Building on this, the team developed an efficient molecular scintillator based on the AIE organic zinc halide complex (TPA-PD)$_2$ZnCl$_2$ (Fig. 4c) [41]. This covalent organic metal halide complex not only exhibited effective X-ray absorption due to the presence of high-Z metal halides but also exhibited rapid and efficient radioluminescence in the solid state thanks to its AIE characteristics. As demonstrated in Fig. 4d, e, (TPA-PD)$_2$ZnCl$_2$ exhibited good radiation stability, remaining stable after 36 on–off cycles, and achieved a remarkably low detection limit of 80.23 nGy s^{-1}, making it one of the most efficient molecular scintillators developed to date.

In another significant study, Liu's team developed a densely structured and rigid metal–organic gel scintillator, YTU-G-1 (Fig. 4f), incorporating the AIE-active molecule H$_4$TCPE [42]. As shown in Fig. 4g, this innovative scintillator demonstrates a high quantum efficiency of 95.5% and

an exceptionally low radiation detection limit of 41 nGy s^{-1}, highlighting the continued advancements of AIE materials in the field of radiation detection.

Importantly, the application of AIE materials extends beyond small molecules and metal-doped complexes. For instance, Tanaka et al. [43] developed a film-type scintillator based on conjugated polymers with AIE properties (Fig. 4h). The team synthesized a series of boron diimide copolymers, varying the substituents and comonomers to optimize performance. These polymers not only exhibited characteristic AIE behavior but also emitted distinct luminescence colors under X-ray excitation, a crucial feature for detecting radiation across different energy levels. This advancement underscores the versatility of AIE materials in X-ray detection and imaging.

Table 1 summarized the radiation detection properties of representative aggregation-induced emissive scintillators. Compared with the traditional organic and inorganic scintillators, AIE materials possess unique properties, including efficient X-ray absorption, high light yield, and low detection limits [44–53]. For instance, while inorganic scintillators such as SrI$_2$:Eu exhibit a high light yield of 93,000 photons/MeV, they suffer from relatively long decay times (1200 ns), limiting their performance in fast response applications [49]. In contrast, AIE scintillators like TPE-4Br, despite their lower light yield of 34,600 photons MeV^{-1}, demonstrate a significantly faster decay time of 1.79 ns and a high PLQY of 93.7%. This combination of rapid response and high quantum yield ensures superior detection efficiency. In addition, AIE materials also offer immense potential for performance optimization through tunable molecular structures, making them potential candidates for next-generation radiation detection technologies.

3.2 Radiation Imaging

X-ray imaging is a technique that leverages the ability of X-rays to penetrate objects and their subsequent detection to generate detailed images of the internal structures of those objects [54–58]. This technology is widely used in various fields, including medical diagnostics, industrial inspection, security screening, and scientific research [59–61]. AIE materials, which exhibit enhanced luminescence in their aggregated state, offer advantages such as simple synthesis,
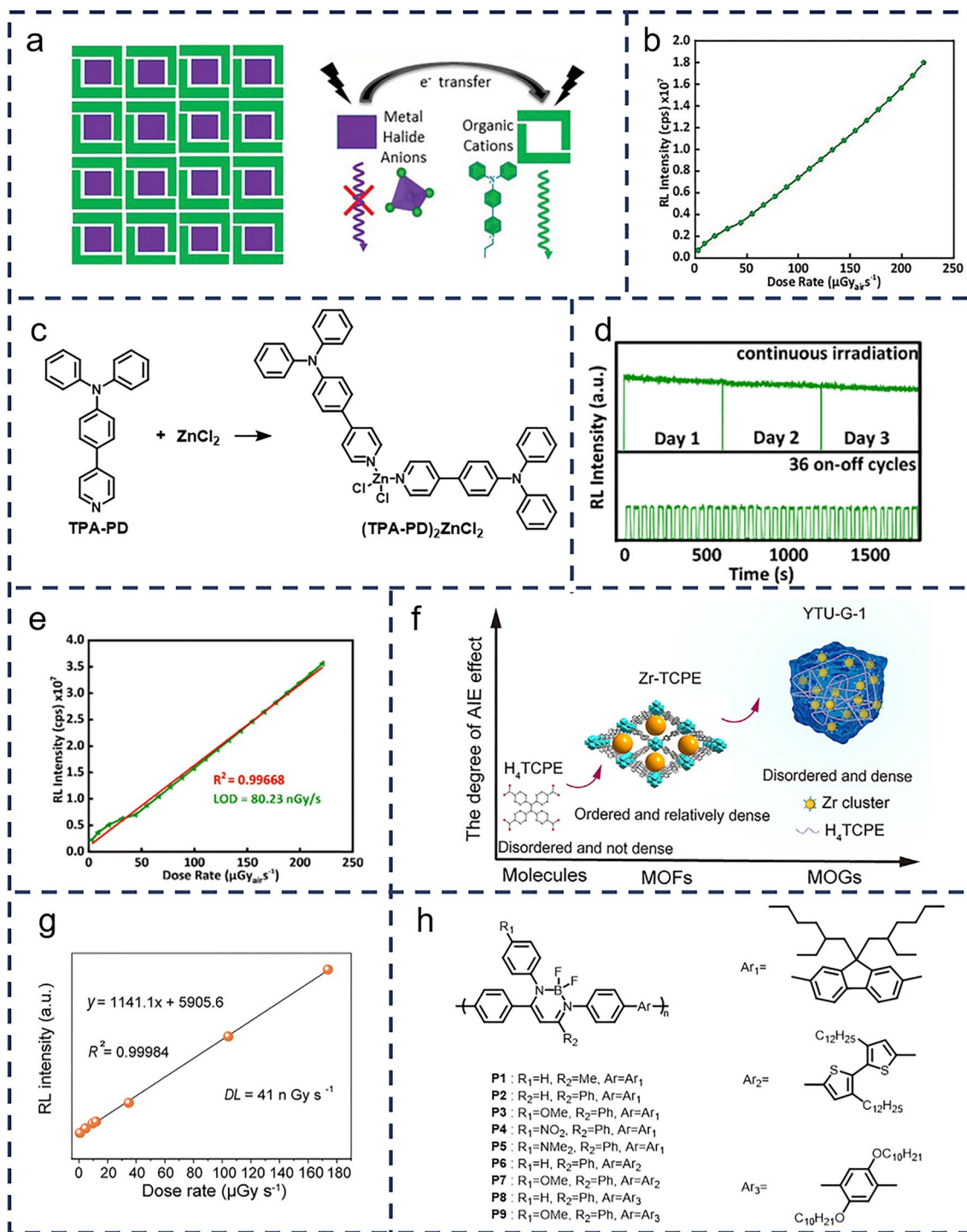
Fig. 4 **a** Design of a 0D organic metal halide hybrid containing metal halide polyhedrons ($ZnBr_4^{2-}$, purple squares) fully isolated and surrounded by AIE organic cations (TPA-P$^+$, green rectangles), and mechanism of sensitized radioluminescence. **b** Dependence of radioluminescence on the radiation dose rate for (TPA-P)$_2$ZnBr$_4$. (**a** and **b** Reproduced with permission from Ref. [40] Copyright 2023 Wiley–VCH GmbH). **c** AIE organic molecule 4-(4-(diphenylamino)phenyl)-1-(propyl)pyridinium (TPA-PD) reacts with zinc chloride (ZnCl$_2$) to form the organometallic metal halide complex (TPA-PD)$_2$ZnCl$_2$. **d** Radioluminescence stability at 448 nm for (TPA-PD)$_2$ZnCl$_2$ under continuous irradiation (top) and repeated on–off cycles of X-rays (bottom) at a dose rate of 221.39 μGy s^{-1}; **e** Dose–response linearity measurement of (TPA-PD)$_2$ZnCl$_2$. (**d** and **e** Reproduced with permission from Ref. [41] Copyright 2024 The Royal Society of Chemistry). **f** Construction of highly luminescent metal organogel (MOG), YTU-G-1; **g** Normalized radioluminescence intensity with different X-ray dose rates for YTU-G-1 in which the slope represents the sensitivity for X-ray. (**f** and **g** Reproduced with permission from Ref. [42] Copyright 2024 Elsevier Inc). **h** A series of boron diimide copolymers with different substituents and comonomers synthesized by Suzuki–Miyaura coupling

Table 1 Some systems containing AIE molecules have excellent radiation detection properties.

AIE molecule included	Light yield (photons MeV^{-1})	τ_{PL}(ns)	PLQY (%)	Limit of detection (nGy s^{-1})	References
HPS	11,000	6.2	[1]72.3	–	[37, 38]
TPE-4Br	34,600	1.79	93.7	109	[39]
TPA-P$^+$	14,700 ± 800	9.96	71	21.3	[40]
TPA-PD	13,423	1.81	65	80.23	[41]
H$_4$TCPE	–	4.10	95.5	41	[42]
(BODIPY polymer)	–	[2]0.57	[2]11	–	[43]
H$_4$ETTC	–	1.73	95.5	44	[53]

Table 1 (continued)

AIE molecule included	Light yield (photons MeV^{-1})	τ_{PL}(ns)	PLQY (%)	Limit of detection (nGy s^{-1})	References
OBP	–	7.2×10^3	90	34.6	[54]

[1] 10 mol% HPS-doped PVK

[2] Data from polymer P1

low cost, and high fluorescence quantum yield. These properties significantly improve imaging quality by increasing signal intensity, while their short fluorescence lifetime enhances temporal resolution and the signal-to-noise ratio
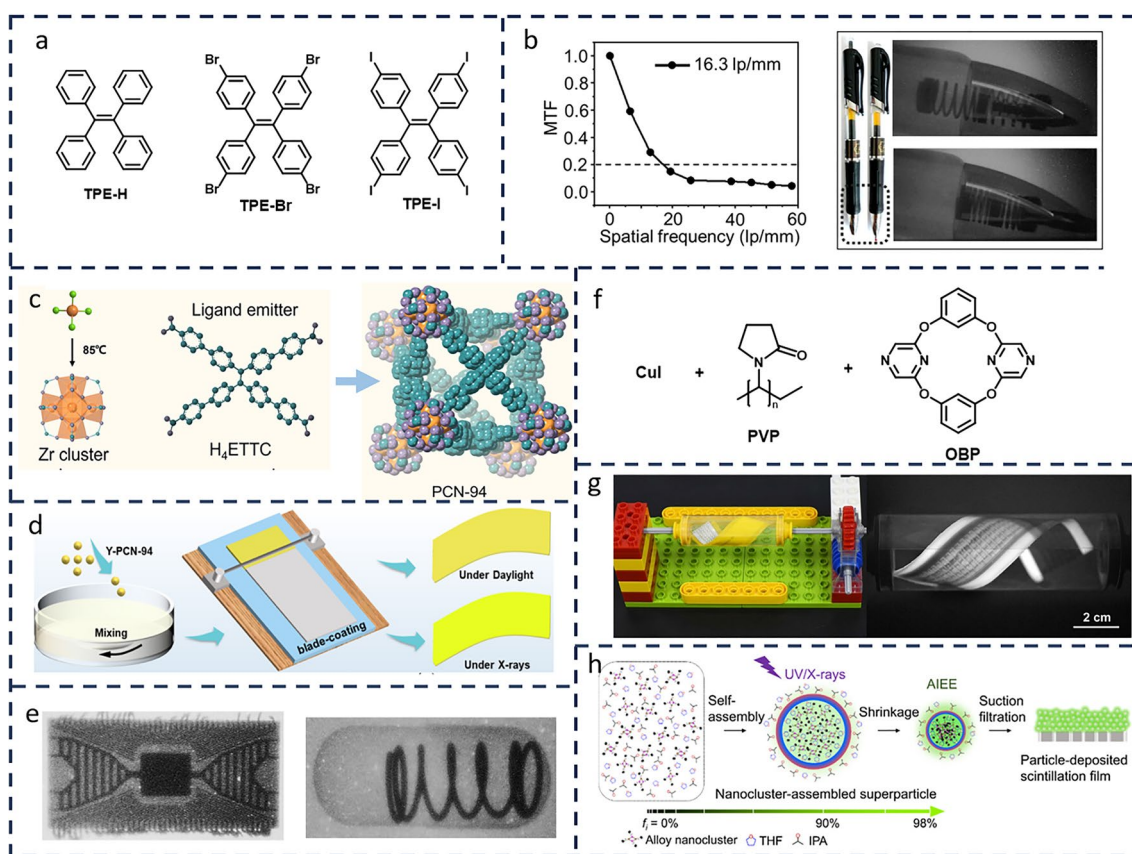

Fig. 5 **a** A range of AIE materials containing halogen atoms: TPE-H, TPE-Br, TPE-I. **b** Modulation transfer function (MTF) of TPE-Br film X-ray image (PSF: 10 wt% of the composite) (left), bright and dark field photos of the pen (right). (**b** Reproduced with permission from Ref. [62] Copyright 2022 American Chemical Society). **c** PCN-94 crystal structure formed by Zr clusters and the organic ligand H$_4$ETTC. **d** Schematic representation of the preparation of the composite Y-PCN-94@PDMS membrane. **e** X-ray imaging of a chipboard (left) and a spring-loaded pill (right) by using the composite Y-PCN-94@PDMS scintillating membrane. (**c–e** Reproduced with permission from Ref. [63] Copyright 2023 American Chemical Society). **f** Molecular structures contained in metal–organic framework (MOF) scintillators based on copper iodide clusters. **g** Dynamic flexible X-ray imaging device and real-time imaging photographs of flexible OLED display. (**g** Reproduced with permission from Ref. [64] Copyright 2023 Wiley–VCH GmbH). **h** Novel 0D scintillator Cu$_2$Au$_2$(R-BTT)$_4$ based on phosphorescent AIEE-active metal nanoclusters and its particle deposition scintillation film preparation process. (**h** Reproduced with permission from Ref. [65] Copyright 2023 American Chemical Society)

of imaging systems. As a result, AIE materials hold great promise for advancing radiation imaging technologies.

Due to the challenges associated with the practical use of powder samples in X-ray imaging, researchers have turned to polysulfone (PSF), a highly flexible material, as the substrate. They then doped a series of halogen-containing AIE materials to create thin films suitable for X-ray imaging applications (Fig. 5a) [62]. As shown in Fig. 5b (left), the resulting film achieved an impressive X-ray imaging resolution of 16.3 lp mm^{-1}, making it a promising candidate for X-ray photography and security screening. Furthermore, the TPE-Br scintillator screen demonstrated clear visibility of the internal structure of steel springs inside a pen (Fig. 5b, right).

The lack of high atomic number components limits the ability of some materials to effectively block X-rays, resulting in weak X-ray absorption and limited light output. To address these limitations, new scintillator materials or strategies must be developed. One promising direction is the design of organic–inorganic hybrid multi-component scintillators. For instance, Zhang et al. [63] reported a flexible composite scintillating film with excellent imaging performance. This film was created by embedding AIE luminophore (H$_4$ETTC)-functionalized MOF scintillators (Y-PCN-94) into a polymer matrix (PDMS) (Fig. 5c). Notably, Y-PCN-94 demonstrates a strong AIE effect under both UV and X-ray irradiation, marking the first observation of AIE behavior in a MOF system under ionizing radiation. Combining the AIE effect with strong X-ray blocking ability, this material exhibits outstanding radioluminescence characteristics, such as a low X-ray detection limit (1.6 µGy s^{-1}) and high imaging resolution (> 14.3 lp mm^{-1}). The authors also fabricated a flexible composite X-ray scintillating film using PDMS and Y-PCN-94 through a simple blade-coating technique. In this Y-PCN-94@PDMS composite film, the internal components of wood chips and spring balls can be clearly displayed (Fig. 5d, e). Similarly, Peng et al. [64] developed an AIE-characteristic cyclic bridge ligand iodinated copper cluster MOF scintillator (Fig. 5f) with high X-ray excited luminescence (XEL) efficiency and excellent chemical stability. By adding PVP to prepare regular rod-shaped microcrystals, both XEL and processability were enhanced. This microcrystal was then used to fabricate a flexible scintillator screen capable of high-performance X-ray imaging in humid environments, achieving dynamic flexible X-ray imaging for the first time, with a resolution as high as 20 lp mm^{-1}. This system enables real-time monitoring of the internal structure

of flexible objects (Fig. 5g). Huang et al. [65] also explored a new class of 0D scintillators based on phosphorescent AIEE-active metal nanoclusters, Cu$_2$Au$_2$(R-BTT)$_4$, and prepared particle-deposited scintillating films of varying thicknesses, achieving a spatial resolution as high as 28.4 lp mm^{-1}.

4 Applications of AIE Scintillators in Other Radiation Detection

4.1 γ-Ray Detection

γ rays, the electromagnetic waves with the shortest wavelengths, possess the highest photon energy, ranging from thousands of electron volts to approximately 8 million electron volts, and exhibit the strongest penetrating ability. Due to these properties, γ-rays are widely used in applications such as interplanetary exploration, non-contact industrial sensors, and cancer therapy [66, 67]. When γ-rays pass through a detector, they may be absorbed, scattered, or interact with the detector material through Compton scattering. This interaction produces signals like scintillation light and charge carriers, which are then converted into electrical signals and recorded [68]. Traditional γ-ray detectors, typically based on scintillating crystals or high-performance semiconductor materials [69–71], such as NaI(Tl) and CdZnTe, offer high detection efficiency. However, these materials often come with complex fabrication processes, high costs, and limited flexibility.

In response to these limitations, AIE materials, recognized for their superior optical properties, have emerged as promising candidates for novel γ-ray detection materials. Liu et al. [72] successfully developed a simple fluorescent detection technique based on the principle of aggregation-induced emission (AIE) for γ-ray detection. As illustrated in Fig. 6a, this technique exploits the AIE characteristics of siloxane compound 1 and the vulnerability of the sulfonyl groups (-SO$_2$-) in the main chain of polymer 2 to degradation under γ-ray irradiation, enabling effective γ-ray detection. Furthermore, this detection method operates under ambient conditions and can sensitively detect γ-ray doses as low as 0.13 kGy (Fig. 6b). Under γ radiation, halogenated solvents such as chloroform (CHCl$_3$) and dichloromethane (CH$_2$Cl$_2$) decompose into free radicals [73, 74]. These radicals are highly reactive and quickly recombine to form new compounds, including hydrochloric acid (HCl). Notably, water (humidity) and oxygen in ambient conditions have little
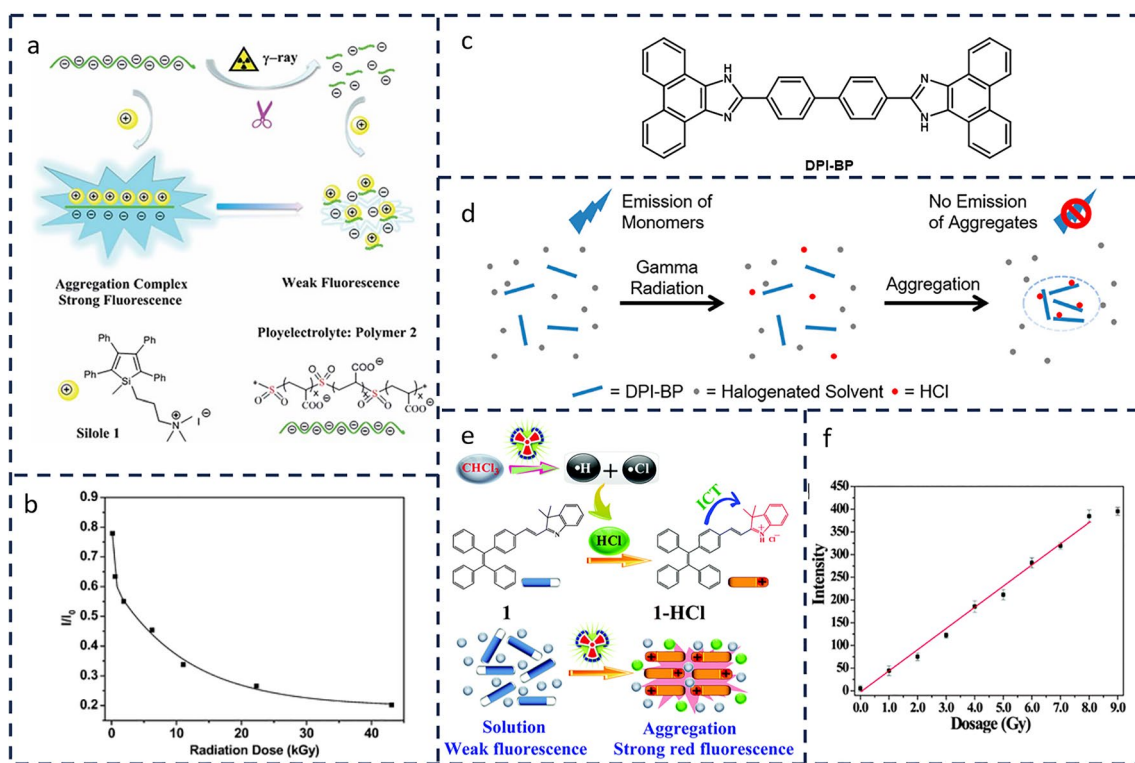
Fig. 6 **a** γ-ray fluorescence detection design based on silicene 1 and polymer 2. **b** Variation of fluorescence intensity at 465 nm of the aqueous solution of silole 1 (1.0×10^{-5} M) and polymer 2 (15 mg L^{-1}) with increasing γ-ray radiation dose. (**a** and **b** Reproduced with permission from Ref. [72] Copyright 2011 The Royal Society of Chemistry). **c** Molecular structure of DPI-BP. **d** Schematic drawing of the fluorescence sensing mechanism of DPI-BP. Protonation interaction with HCl generated by radiation causes molecular aggregation of DPI-BP, leading to fluorescence quenching due to π–π stacking. (**d** Reproduced with permission from Ref. [78] Copyright 2014 American Chemical Society). **e** Chemical structures of compound 1 and 1·HCl and design rationale for the fluorescence turn-on detection of γ-radiation. **f** A plot showing the fluorescence intensity at 640 nm *vs.* the dosage of γ-rays for the $CHCl_3$ solution of 1 (3.0 mL, 10.0 μM); the data in the range of 0.0–8.0 Gy were fitted using the following equation: $Y = 46.37351X - 6.48515$, $R^2 = 0.991$. (**e** and **f** Reproduced with permission from Ref. [79] Copyright 2015 The Royal Society of Chemistry)

effect on HCl production because their reactions with free radicals are slow [75–77].

Building on this principle, Zang et al. [78] developed a novel fluorescent sensor molecule, DPI-BP (Fig. 6c), with a sensing mechanism primarily based on the addition reaction between HCl and the imidazole groups of DPI-BP. As shown in Fig. 6d, the HCl adduct of DPI-BP undergoes aggregation, leading to the quenching of its molecular fluorescence due to intermolecular π-π stacking. This aggregation allows the sensor to rapidly detect the HCl produced under γ radiation. The sensor significantly enhances the detection limit of γ radiation by three orders of magnitude, reducing it to 0.01 Gy. Building on this, Dong et al. [79] harnessed the AIE characteristics of the TPE unit in combination with the chemical behavior of $CHCl_3$, which decomposes to generate

HCl under γ-ray irradiation. This protonates compound 1 and promotes its aggregation, yielding a γ radiation detection limit of 0.023 Gy, thus enabling highly sensitive γ-ray detection (Fig. 6e, f).

The key advantage of AIE materials in γ-ray detection lies in their ability to enhance the detection response through molecular design. Additionally, the low cost and solution processability of AIE materials make them attractive candidates for large-scale γ-ray detectors, especially for portable and flexible designs—an important factor for practical applications.
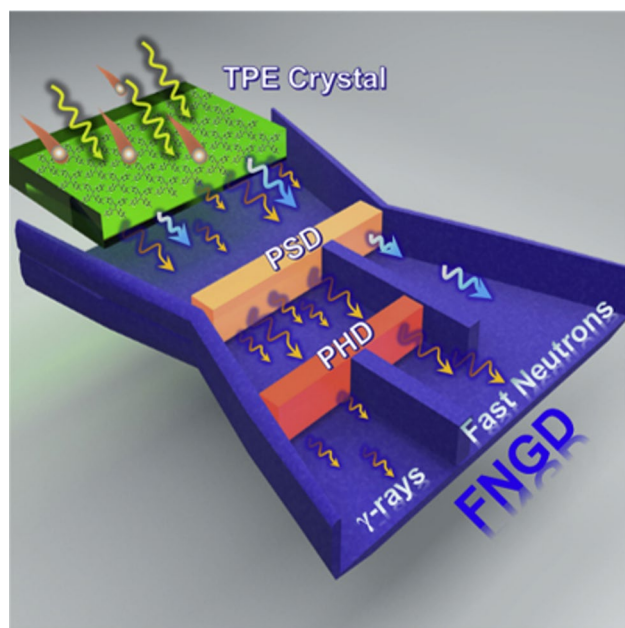
Fig. 7 Schematic of fast neutron/γ discrimination with TPE single crystal. (Reproduced with permission from Ref. [85] Copyright 2022 Elsevier Inc.)

4.2 Fast Neutron Detection

The principle behind fast neutron detection relies on the interaction between high-energy fast neutrons and hydrogen nuclei in the scintillator material. After passing through the target object, fast neutrons undergo elastic scattering with hydrogen nuclei, resulting in recoil protons. These recoil protons deposit energy in the scintillator, which in turn generates electron–hole pairs, leading to the excitation of the scintillator and the emission of visible fluorescence. This process effectively converts the neutron field distribution into a visible light pattern, which is subsequently captured and recorded by the optical system, enabling fast neutron detection and imaging [80]. Due to their strong penetrating power, fast neutrons can traverse most materials, making fast neutron detection a promising technique for non-destructive testing of large components. This technology holds significant potential in various fields, including aerospace, nuclear energy, and advanced manufacturing [81–84].

In this context, Sun et al. [85] introduced a "dual discrimination" concept using TPE-based single-crystal scintillators (Fig. 7) to effectively distinguish fast neutrons from the accompanying γ noise. By employing pulse shape discrimination (PSD) and pulse height discrimination (PHD), they achieved a high level of separation between fast neutrons and γ rays, thereby enhancing the fast neutron count rate.

The application of AIE materials in fast neutron detection is still in its early stages but shows considerable promise. A key challenge lies in designing AIE molecules optimized for neutron detection, particularly with high hydrogen content, as hydrogen atoms efficiently interact with fast neutrons. Neutron detection also demands materials with high radiation stability, as exposure to high-energy particles like fast neutrons can cause significant damage.

To address these challenges, integrating AIE materials with neutron-absorbing components, such as boron or lithium, or designing hydrogen-rich AIE molecules can enhance their interaction with fast neutrons. This interaction generates secondary particles, such as alpha particles or protons, which excite the AIE materials to emit detectable fluorescence signals. The chemical tunability of AIE materials further enables molecular engineering to optimize their neutron interaction efficiency and optical response, improving overall detector performance. Compared to traditional detectors, AIE-based systems offer the potential for superior stability, higher sensitivity, and adaptability to complex detection environments, positioning them as promising candidates for next-generation neutron detection technologies.

5 Conclusions and Prospects

The unique properties of AIE materials have led to revolutionary advancements in the field of radiation detection and imaging. Unlike traditional luminescent materials, AIE materials exhibit enhanced luminescence efficiency in their aggregated state, offering significant advantages for various applications, including X-ray, γ-ray, fast neutron detection, and radiation imaging. Furthermore, the chemical diversity of AIE materials provides vast opportunities for designing novel detectors. By utilizing strategies such as molecular structure optimization, metal doping, and polymer incorporation, it is possible to develop detectors with superior AIE-based radiation detection capabilities. This advances radiation detection technology toward higher sensitivity, resolution, and stability.

However, despite these promising advancements, several challenges need to be addressed. The stability of AIE materials under prolonged exposure to high-energy radiation, such as X-rays and γ-rays, remains a critical concern. Accumulation of radiation-induced defects can quench luminescence and degrade performance, particularly in comparison to the inherent robustness of traditional inorganic scintillators. Additionally, while AIE materials exhibit high photoluminescence quantum yields and short lifetimes, their light yield has yet to surpass that of conventional organic and inorganic scintillators, limiting their competitiveness in applications requiring high sensitivity and resolution. Challenges in fabrication, including poor film formation, non-uniformity, and scalability, also hinder their development for large-area detectors. Furthermore, enhancing detection capabilities for challenging radiation types, such as fast neutrons and α particles, remains an area requiring further exploration.

Looking ahead, the future of AIE materials in radiation detection lies in advancing molecular design strategies and exploring novel composite systems. Strategies such as optimizing molecular structures, incorporating metal doping, and integrating AIE-active molecules with stable inorganic components can improve radiation tolerance, mitigate luminescence degradation, and enhance overall performance. Additionally, developing scalable and cost-effective fabrication methods, such as inkjet printing or spray-coating, will facilitate the production of large-area detectors with consistent properties. Exploring multifunctional materials and hybrid systems will further expand detection capabilities, offering solutions for diverse and complex radiation environments. Continued progress in material science and detection technologies will position AIE materials as pivotal components in next-generation radiation detection systems, addressing critical needs in health monitoring, security screening, and scientific research.

Author Contributions Yuting Gao contributed to conceptualization, supervision, funding acquisition, writing—review & editing. Xinyi Li done investigation, writing—original draft. Guangda Niu helped in funding acquisition, writing—review & editing. Jiafu Yu, Yinghao Fan done investigation, writing—review.

Declarations

References

1. K.R. Dudipala, T.-H. Le, W. Nie, R.L.Z. Hoye, Halide perovskites and their derivatives for efficient, high-resolution direct radiation detection: design strategies and applications. Adv. Mater. **36**, 2304523 (2024). https://doi.org/10.1002/adma.202304523

2. Y.J. Heo, K.T. Kim, M.J. Han, C.W. Moon, J.E. Kim et al., Development of a stable and sensitive semiconductor detector by using a mixture of lead(II) iodide and lead monoxide for NDT radiation dose detection. J. Inst. **13**, C03023 (2018). https://doi.org/10.1088/1748-0221/13/03/c03023

3. M. Inês Silva, E. Malitckii, T.G. Santos, P. Vilaça, Review of conventional and advanced non-destructive testing techniques for detection and characterization of small-scale defects. Prog. Mater. Sci. **138**, 101155 (2023). https://doi.org/10.1016/j.pmatsci.2023.101155

4. I. Høiaas, K. Grujic, A.G. Imenes, I. Burud, E. Olsen et al., Inspection and condition monitoring of large-scale photovoltaic power plants: a review of imaging technologies. Renew. Sustain. Energy Rev. **161**, 112353 (2022). https://doi.org/10.1016/j.rser.2022.112353

5. G.F. Knoll, *Radiation Detection and Measurement* (John Wiley & Sons, New Jersey, 2010)

6. J. Oliveira, V. Correia, P. Costa, A. Francesko, G. Rocha et al., Stretchable scintillator composites for indirect X-ray detectors. Compos. Part B Eng. **133**, 226–231 (2018). https://doi.org/10.1016/j.compositesb.2017.09.031

7. L.C. Andrews, R.L. Phillips, C.Y. Hopen, M.A. Al-Habash, Theory of optical scintillation. J. Opt. Soc. Am. A **16**, 1417 (1999). https://doi.org/10.1364/josaa.16.001417

8. Y. He, J. Song, M. Li, K. Sakhatskyi, W. Li et al., Perovskite computed tomography imager and three-dimensional reconstruction. Nat. Photonics **18**, 1052–1058 (2024). https://doi.org/10.1038/s41566-024-01506-y

9. C.L. Melcher, Scintillation crystals for PET. J. Nuclear Med. **41**, 1051–1055 (2000)

10. J. Chen, L. Zhang, R. Zhu, Large size LSO and LYSO crystal scintillators for future high-energy physics and nuclear physics experiments. Nucl. Instrum. Meth. Phys. Res. Sect. A Accel. Spectrometers, Detect. Assoc. Equip. **572**(1), 218–224 (2007). https://doi.org/10.1016/j.nima.2006.10.213

11. Y.G. Zdesenko, F.T. Avignone, V.B. Brudanin, F.A. Danevich, S.S. Nagorny et al., Scintillation properties and radioactive contamination of $CaWO_4$ crystal scintillators. Nucl. Instrum. Meth. Phys. Res. Sect A Accel. Spectrometers Detect. Assoc. Equip. **538**, 657–667 (2005). https://doi.org/10.1016/j.nima.2004.09.030

12. S. Yamamoto, H. Tomita, Comparison of light outputs, decay times, and imaging performance of a ZnS(Ag) scintillator for alpha particles, beta particles, and gamma photons. Appl. Radiat. Isot. **168**, 109527 (2021). https://doi.org/10.1016/j.apradiso.2020.109527

13. Z. Tan, J. Pang, G. Niu, J.-H. Yuan, K.-H. Xue et al., Tailoring the electron and hole dimensionality to achieve efficient and stable metal halide perovskite scintillators. Nanophotonics **10**, 2249–2256 (2021). https://doi.org/10.1515/nanoph-2020-0624

14. P. Yang, C.D. Harmon, F.P. Doty, J.A. Ohlhausen, Effect of humidity on scintillation performance in Na and Tl activated CsI crystals. IEEE Trans. Nucl. Sci. **61**, 1024–1031 (2014). https://doi.org/10.1109/TNS.2014.2300471

15. I. Holl, E. Lorenz, G. Mageras, A measurement of the light yield of common inorganic scintillators. IEEE Trans. Nucl. Sci. **35**, 105–109 (1988). https://doi.org/10.1109/23.12684

16. T. Yanagida, M. Koshimizu, G. Okada, T. Kojima, J. Osada et al., Comparative study of nondoped and Eu-doped SrI_2 scintillator. Opt. Mater. **61**, 119–124 (2016). https://doi.org/10.1016/j.optmat.2016.05.030

17. L. Viererbl, A. Kolros, H.A. Vratislavská, Long-term afterglow of solid scintillators. Radiat. Prot. Dosimetry **198**, 666–669 (2022). https://doi.org/10.1093/rpd/ncac116

18. G.V. Bünau, J.B. Birks, photophysics of aromatic molecules. Wiley-interscience, London 1970.704 seiten. preis: 210s. Ber. Der Bunsengesellschaft Für Phys. Chem. **74**, 1294–1295 (1970). https://doi.org/10.1002/bbpc.19700741223

19. J. Luo, Z. Xie, J.W. Lam, L. Cheng, H. Chen et al., Aggregation-induced emission of 1-methyl-1, 2, 3, 4, 5-pentaphenylsilole. Chem. Commun. 1740–1741 (2001). https://doi.org/10.1039/b105159h

20. P. Han, C. Lin, E. Xia, J. Cheng, Q. Xia et al., Non-doped blue AIEgen-based OLED with EQE approaching 10.3 %. Angew. Chem. Int. Ed. **62**, 202310388 (2023). https://doi.org/10.1002/anie.202310388

21. S. Du, M. Luo, D. Li, L. Lyu, W. Li et al., Hot-exciton mechanism and AIE effect boost the performance of deep-red emitters in non-doped OLEDs. Adv. Mater. **35**, e2303304 (2023). https://doi.org/10.1002/adma.202303304

22. J. Lou, G. Li, X. Guo, B. Li, D. Yang et al., Creation of high-quality deep-blue AIE emitter with a crossed long-short axis structure for efficient and versatile OLEDs. Small **20**, 2308468 (2024). https://doi.org/10.1002/smll.202308468

23. V. Kachwal, J.-C. Tan, Stimuli-responsive electrospun fluorescent fibers augmented with aggregation-induced emission (AIE) for smart applications. Adv. Sci. **10**, e2204848 (2022). https://doi.org/10.1002/advs.202204848

24. Z. Yang, P.-A. Cazade, J.-L. Lin, Z. Cao, N. Chen et al., High performance mechano-optoelectronic molecular switch. Nat. Commun. **14**, 5639 (2023). https://doi.org/10.1038/s41467-023-41433-0

25. N.L. Leung, N. Xie, W. Yuan, Y. Liu, Q. Wu et al., Restriction of intramolecular motions: the general mechanism behind aggregation-induced emission. Chemistry **20**, 15349–15353 (2014). https://doi.org/10.1002/chem.201403811

26. Y. Chen, J.W.Y. Lam, R.T.K. Kwok, B. Liu, B.Z. Tang, Aggregation-induced emission: fundamental understanding and future developments. Mater. Horiz. **6**, 428–433 (2019). https://doi.org/10.1039/C8MH01331D

27. A.M. Fraind, J.D. Tovar, Comparative survey of conducting polymers containing benzene, naphthalene, and anthracene cores: interplay of localized aromaticity and polymer electronic structures. J. Phys. Chem. B **114**, 3104–3116 (2010). https://doi.org/10.1021/jp9101459

28. F. Song, Z. Xu, Q. Zhang, Z. Zhao, H. Zhang et al., Highly efficient circularly polarized electroluminescence from aggregation-induced emission luminogens with amplified chirality and delayed fluorescence. Adv. Funct. Mater. **28**, 1800051 (2018). https://doi.org/10.1002/adfm.201800051

29. M.-S. Yuan, D.-E. Wang, P. Xue, W. Wang, J.-C. Wang et al., Fluorenone organic crystals: two-color luminescence switching and reversible phase transformations between π–π stacking-directed packing and hydrogen bond-directed packing. Chem. Mater. **26**, 2467–2477 (2014). https://doi.org/10.1021/cm500441r

30. Z. Zhao, P. Lu, J.W.Y. Lam, Z. Wang, C.Y.K. Chan et al., Molecular anchors in the solid state: restriction of intramolecular rotation boosts emission efficiency of luminogen aggregates to unity. Chem. Sci. **2**, 672–675 (2011). https://doi.org/10.1039/C0SC00521E

31. S.-Y. Yang, J. Wang, Z. Deng, Y. Xu, X. Su et al., Spiro-materials with aggregation-induced emission. Matter **7**, 3390–3421 (2024). https://doi.org/10.1016/j.matt.2024.07.017

32. R. Chen, Z. Li, C. Peng, L. Wen, L. Xiao et al., Rational design of novel lipophilic aggregation-induced emission probes for revealing the dynamics of lipid droplets during lipophagy and ferroptosis. Anal. Chem. **94**, 13432–13439 (2022). https://doi.org/10.1021/acs.analchem.2c02260

33. J. Zhang, L. Hu, K. Zhang, J. Liu, X. Li et al., How to manipulate through-space conjugation and clusteroluminescence of simple AIEgens with isolated phenyl rings. J.

Am. Chem. Soc. **143**, 9565–9574 (2021). https://doi.org/10.1021/jacs.1c03882

34. J.C. Koziar, D.O. Cowan, Photochemical heavy-atom effects. Acc. Chem. Res. **11**, 334–341 (1978). https://doi.org/10.1021/ar50129a003

35. M.N. Berberan Santos, External heavy-atom effect on fluorescence kinetics. Phys. Chem. Commun. **3**, 18 (2000). https://doi.org/10.1039/b002307h

36. A. Pietropaolo, M. Angelone, R. Bedogni, N. Colonna, A.J. Hurd et al., Neutron detection techniques from μeV to GeV. Phys. Rep. **875**, 1–65 (2020). https://doi.org/10.1016/j.physrep.2020.06.003

37. A. Sato, M. Koshimizu, Y. Fujimoto, S. Komatsuzaki, S. Kishimoto et al., Novel class of organic crystal scintillators based on aggregation-induced emission. Mater. Chem. Front. **6**, 1470–1476 (2022). https://doi.org/10.1039/d2qm00187j

38. A. Sato, M. Koshimizu, Y. Fujimoto, K. Asai, Development of plastic scintillators doped with silole-based aggregation-induced emission phosphors for scintillation light yield improvement. Opt. Mater. **136**, 113493 (2023). https://doi.org/10.1016/j.optmat.2023.113493

39. X. Du, S. Zhao, L. Wang, H. Wu, F. Ye et al., Efficient and ultrafast organic scintillators by hot exciton manipulation. Nat. Photon. **18**, 162–169 (2024). https://doi.org/10.1038/s41566-023-01358-y

40. T.B. Shonde, M. Chaaban, H. Liu, O.J. Olasupo, A. Ben-Akacha et al., Molecular sensitization enabled high performance organic metal halide hybrid scintillator. Adv. Mater. **35**, e2301612 (2023). https://doi.org/10.1002/adma.202301612

41. T.B. Shonde, H. Liu, O.J. Olasupo, A. Bouchard, S. Bouchard et al., Aggregation-induced emission organic metal halide complex for X-ray scintillation. Mater. Horiz. **11**, 3076–3081 (2024). https://doi.org/10.1039/d4mh00142g

42. X. Wang, X. Wang, J. Song, H. Bao, M. Yuan et al., Anchoring the AIEgen by Zr clusters in metal-organic gel for efficient X-ray detection and imaging. Chem **10**, 1268–1278 (2024). https://doi.org/10.1016/j.chempr.2024.01.024

43. K. Tanaka, T. Yanagida, A. Hirose, H. Yamane, R. Yoshii et al., Synthesis and color tuning of boron diiminate conjugated polymers with aggregation-induced scintillation properties. RSC Adv. **5**, 96653–96659 (2015). https://doi.org/10.1039/C5RA20459C

44. L. Lopez, P. Pichon, P. Loiseau, B. Viana, R. Mahiou et al., Ce: LYSO, from scintillator to solid-state lighting as a blue luminescent concentrator. Sci. Rep. **13**, 7199 (2023). https://doi.org/10.1038/s41598-023-32689-z

45. H. Xu, W. Liang, Z. Zhang, C. Cao, W. Yang et al., 2D perovskite Mn^{2+}-doped $Cs_2CdBr_2Cl_2$ scintillator for low-dose high-resolution X-ray imaging. Adv. Mater. **35**, e2300136 (2023). https://doi.org/10.1002/adma.202300136

46. P. Lecoq, Development of new scintillators for medical applications. Nucl. Instrum. Meth. Phys. Res. Sect A Accel. Spectrometers Detect. Assoc. Equip. **809**, 130–139 (2016). https://doi.org/10.1016/j.nima.2015.08.041

47. J. Glodo, K.S. Shah, M. Klugerman, P. Wong, B. Higgins et al., Scintillation properties of LuI_3: Ce. Nucl. Instrum. Meth. Phys. Res. Sect A Accel. Spectrometers Detect. Assoc. Equip. **537**, 279–281 (2005). https://doi.org/10.1016/j.nima.2004.08.026

48. W.W. Moses, K.S. Shah, Potential for $RbGd_2Br_7$ Ce, $LaBr_3$ Ce, $LaBr_3$ Ce, and LuI_3 Ce in nuclear medical imaging. Nucl. Instrum. Meth. Phys. Res. Sect A Accel. Spectrometers Detect. Assoc. Equip. **537**, 317–320 (2005). https://doi.org/10.1016/j.nima.2004.08.034

49. N.J. Cherepy, G. Hull, A.D. Drobshoff, S.A. Payne, E. van Loef et al., Strontium and barium iodide high light yield scintillators. Appl. Phys. Lett. **92**, 083508 (2008). https://doi.org/10.1063/1.2885728

50. Q. Chen, J. Wu, X. Ou, B. Huang, J. Almutlaq et al., All-inorganic perovskite nanocrystal scintillators. Nature **561**, 88–93 (2018). https://doi.org/10.1038/s41586-018-0451-1

51. F. Maddalena, L. Tjahjana, A. Xie, S.Z. Arramel et al., Inorganic, organic, and perovskite halides with nanotechnology for high–light yield X- and γ-ray scintillators. Crystals **9**, 88 (2019). https://doi.org/10.3390/cryst9020088

52. W. Ma, Y. Su, Q. Zhang, C. Deng, L. Pasquali et al., Thermally activated delayed fluorescence (TADF) organic molecules for efficient X-ray scintillation and imaging. Nat. Mater. **21**, 210–216 (2022). https://doi.org/10.1038/s41563-021-01132-x

53. R. Dhali, D.A.P. Huu, F. Bertocchi, C. Sissa, F. Terenziani, A. Painelli, Understanding TADF: a joint experimental and theoretical study of DMAC-TRZ. Phys. Chem. Chem. Phys. **23**(1), 378–387 (2021). https://doi.org/10.1039/D0CP05982J

54. A.E. Iskandrian, F.G. Hage, *Nuclear cardiac imaging: principles and applications* (Oxford University Press, New York, 2024)

55. W. Alamro, B.C. Seet, Review of practical antennas for microwave and millimetre-wave medical imaging. Electromag. Waves Antenn Biomed. Appl. (2021). https://doi.org/10.1049/PBHE033E_ch6

56. K. Sakhatskyi, B. Turedi, G.J. Matt, E. Wu, A. Sakhatska et al., Stable perovskite single-crystal X-ray imaging detectors with single-photon sensitivity. Nat. Photonics **17**, 510–517 (2023). https://doi.org/10.1038/s41566-023-01207-y

57. J.-X. Wang, L. Gutiérrez-Arzaluz, X. Wang, M. Almalki, J. Yin et al., Nearly 100% energy transfer at the interface of metal-organic frameworks for X-ray imaging scintillators. Matter **5**, 253–265 (2022). https://doi.org/10.1016/j.matt.2021.11.012

58. J.-X. Wang, L. Gutiérrez-Arzaluz, X. Wang, T. He, Y. Zhang et al., Heavy-atom engineering of thermally activated delayed fluorophores for high-performance X-ray imaging scintillators. Nat. Photonics **16**, 869–875 (2022). https://doi.org/10.1038/s41566-022-01092-x

59. N.S. Treister, M.T. Brennan, T.P. Sollecito, B.L. Schmidt, L.L. Patton et al., Exposed bone in patients with head and neck cancer treated with radiation therapy: an analysis of the observational study of dental outcomes in head and neck cancer patients (OraRad). Cancer **128**, 487–496 (2022). https://doi.org/10.1002/cncr.33948

60. R. Booij, N.F. Kämmerling, E.H.G. Oei, A. Persson, E. Tesselaar, Assessment of visibility of bone structures in the wrist using normal and half of the radiation dose with photon-counting detector CT. Eur. J. Radiol. **159**, 110662 (2023). https://doi.org/10.1016/j.ejrad.2022.110662

61. S.S. Khedmatgozar Dolati, P. Malla, J.D. Ortiz, A. Mehrabi, A. Nanni, Identifying NDT methods for damage detection in concrete elements reinforced or strengthened with FRP. Eng. Struct. **287**, 116155 (2023). https://doi.org/10.1016/j.engstruct.2023.116155

62. J.-X. Wang, Y. Wang, I. Nadinov, J. Yin, L. Gutiérrez-Arzaluz et al., Aggregation-induced fluorescence enhancement for efficient X-ray imaging scintillators and high-speed optical wireless communication. ACS Mater. Lett. **4**, 1668–1675 (2022). https://doi.org/10.1021/acsmaterialslett.2c00498

63. L. Zhang, X. Wang, X. Wang, X. Wang, Y. Luo et al., Fabrication of a large-area flexible scintillating membrane for high-resolution X-ray imaging using an AIEgen-functionalized metal-organic framework. Inorg. Chem. **62**, 6421–6427 (2023). https://doi.org/10.1021/acs.inorgchem.3c00381

64. Q.C. Peng, Y.B. Si, J.W. Yuan, Q. Yang, Z.Y. Gao et al., High performance dynamic X-ray flexible imaging realized using a copper iodide cluster-based MOF microcrystal scintillator. Angew. Chem. Int. Ed. **62**, e202308194 (2023). https://doi.org/10.1002/anie.202308194

65. R.-W. Huang, X. Song, S. Chen, J. Yin, P. Maity et al., Radioluminescent Cu–Au metal nanoclusters: synthesis and self-assembly for efficient X-ray scintillation and imaging. J. Am. Chem. Soc. **145**, 13816–13827 (2023). https://doi.org/10.1021/jacs.3c02612

66. S. Yakunin, D.N. Dirin, Y. Shynkarenko, V. Morad, I. Cherniukh et al., Detection of gamma photons using solution-grown single crystals of hybrid lead halide perovskites. Nat. Photonics **10**, 585–589 (2016). https://doi.org/10.1038/nphoton.2016.139

67. A. Goldstein, P. Veres, E. Burns, M.S. Briggs, R. Hamburg et al., An ordinary short gamma-ray burst with extraordinary implications: Fermi-GBM detection of GRB 170817A. Astrophys. J. Lett. **848**, L14 (2017). https://doi.org/10.3847/2041-8213/aa8f41

68. K. Siegbahn, *Alpha- Beta- and Gamma -ray Spectroscopy* (Elsevier, The Netherlands, 2012)

69. F. Liu, R. Wu, J. Wei, W. Nie, A.D. Mohite et al., Recent progress in halide perovskite radiation detectors for gamma-ray spectroscopy. ACS Energy Lett. **7**, 1066–1085 (2022). https://doi.org/10.1021/acsenergylett.2c00031

70. İ Akkurt, F. Waheed, H. Akyildirim, K. Gunoglu, Performance of NaI(Tl) detector for gamma-ray spectroscopy. Indian J. Phys. **96**, 2941–2947 (2022). https://doi.org/10.1007/s12648-021-02210-1

71. A.E. Bolotnikov, K. Ackley, G.S. Camarda, Y. Cui, J.F. Eger et al., High-efficiency CdZnTe gamma-ray detectors. IEEE Trans. Nucl. Sci. **62**, 3193–3198 (2015). https://doi.org/10.1109/tns.2015.2493444

72. Z. Liu, W. Xue, Z. Cai, G. Zhang, D. Zhang, A facile and convenient fluorescence detection of gamma-ray radiation based on the aggregation-induced emission. J. Mater. Chem. **21**, 14487 (2011). https://doi.org/10.1039/c1jm12400e

73. M. Ottolenghi, G. Stein, The radiation chemistry of chloroform. Radiat. Res. **14**, 281 (1961). https://doi.org/10.2307/3570922

74. H.R. Werner, R.F. Firestone, Kinetics of the γ-ray-induced decomposition of Chloroform[1]. J. Phys. Chem. **69**, 840–849 (1965). https://doi.org/10.1021/j100887a023

75. M.M. Kondo, W.F. Jardim, Photodegradation of chloroform and urea using Ag-loaded titanium dioxide as catalyst. Water Res. **25**, 823–827 (1991). https://doi.org/10.1016/0043-1354(91)90162-J

76. C. Kormann, D.W. Bahnemann, M.R. Hoffmann, Photolysis of chloroform and other organic molecules in aqueous titanium dioxide suspensions. Environ. Sci. Technol. **25**, 494–500 (1991). https://doi.org/10.1021/es00015a018

77. H. Shirayama, Y. Tohezo, S. Taguchi, Photodegradation of chlorinated hydrocarbons in the presence and absence of dissolved oxygen in water. Water Res. **35**, 1941–1950 (2001). https://doi.org/10.1016/S0043-1354(00)00480-2

78. J.-M. Han, M. Xu, B. Wang, N. Wu, X. Yang et al., Low dose detection of γ radiation *via* solvent assisted fluorescence quenching. J. Am. Chem. Soc. **136**, 5090–5096 (2014). https://doi.org/10.1021/ja500262n

79. X. Dong, F. Hu, Z. Liu, G. Zhang, D. Zhang, A fluorescent turn-on low dose detection of gamma-radiation based on aggregation-induced emission. Chem. Commun. **51**, 3892–3895 (2015). https://doi.org/10.1039/C4CC10133B

80. K.M. McCall, K. Sakhatskyi, E. Lehmann, B. Walfort, A.S. Losko et al., Fast neutron imaging with semiconductor nanocrystal scintillators. ACS Nano **14**, 14686–14697 (2020). https://doi.org/10.1021/acsnano.0c06381

81. M. Schulz, E. Lehmann, A. Losko, Nondestructive material characterization methods. *Neutron Imaging.* (Elsevier, The Netherlands, 2024)

82. M. Nallaperumal, G.N. Namboodiri, T. Roy, Neutron imaging for aerospace applications. *Neutron Imaging* (Springer, Singapore, 2022)

83. N. Cindro, A survey of fast-neutron reactions. Rev. Mod. Phys. **38**, 391–446 (1966). https://doi.org/10.1103/revmodphys.38.391

84. C. Zeitlin, A.J. Castro, K.B. Beard, M. Abdelmelek, B.M. Hayes et al., Results from the radiation assessment detector on the international space station, part 2: the fast neutron detector. Life Sci. Space Res. **39**, 76–85 (2023). https://doi.org/10.1016/j.lssr.2023.03.005

85. Q. Sun, Z. Hao, J. Li, Z. Liu, H. Wang et al., Dual discrimination of fast neutrons from strong γ noise using organic single-crystal scintillator. Matter **6**, 274–284 (2023). https://doi.org/10.1016/j.matt.2022.10.010